# Behavior and properties of water in silicate melts under deep mantle conditions

**Bijaya Karki** ( bbkarki@lsu.edu )
Louisiana State University
**Dipta B. Ghosh**
Louisiana State University
**Shun-ichiro Karato**
Yale University

**Research Article**

**Keywords:** transport properties of water, hydrous silicate melts, deep mantle conditions

**Posted Date:** March 5th, 2021

**DOI:** https://doi.org/10.21203/rs.3.rs-268378/v1

# Behavior and properties of water in silicate melts under deep mantle conditions

Bijaya B. Karki[1,*], Dipta B. Ghosh[1], Shun-ichiro Karato[2]

[1]*School of Electrical Engineering and Computer Science, Department of Geology and Geophysics, Center for Computation and Technology, Louisiana State University, Baton Rouge, LA 70803, USA*

[2]*Dpeartment of Earth and Planetary Sciences, Yale University, New Haven, CT 06520, USA*

*Corresponding author

## Abstract

Water ($H_2O$) as one of the most abundant fluids present in Earth plays crucial role in the generation and transport of magmas in the interior. Though hydrous silicate melts have been studied extensively, the experimental data are confined to relatively low pressures and the computational results are still rare. Moreover, these studies imply large differences in the way water influences the physical properties of silicate magmas, such as density and electrical conductivity. Here, we invesigate the equation of state, speciation, and transport properties of water dissolved in $Mg_{1-x}Fe_xSiO_3$ and $Mg_{2(1-x)}Fe_{2x}SiO_4$ melts (for $x$ = 0 and 0.25) as well as in its bulk (pure) fluid state over the entire mantle pressure regime at 2000 to 4000 K using first-principles molecular dynamics. The simulation results allow us to constrain the partial molar volume of the water component in melts along with the molar volume of pure water. The predicted volume of silicate melt+water solution is negative at low pressures but becomes zero above 15 GPa implying ideal mixing at higher pressures. Consequently, the hydrous component tends to lower the melt density to similar extent over much of the mantle pressure regime irrespective of composition. Our results also show that hydrogen diffuses fast in silicate melts and enhances the melt electrical conductivity in a way that differs from electrical conduction in the bulk water. The speciation of the water component varies considerably from the bulk water structure as well. Water is dissolved in melts mostly as hydroxyls at low pressure and as -O-H-O-, -O-H-O-H- and other extended species with increasing pressure. On the other hand, the pure water behaves as a molecular fluid below 15 GPa, gradually becoming a dissociated fluid with further compression. On the basis of modeled density and conductivity results, we suggest that partial melts containing a few percent of water may be gravitationally trapped both above and below the upper mantle-transition region. Moreover, such hydrous melts can give rise to detectable electrical conductance by means of electromagnetic sounding observations.

## Introduction

The Earth's mantle is thought to contain large amounts of water. Although the majority of water (hydrogen) in the mantle is in minerals, water in silicate melts also plays a key role in global water cycle[1-3]. During the accretion state, large-scale magma ocean may have served as a reservoir of volatiles including water delivered to Earth. In the later stages of Earth evolution, melting is limited, mostly existing as partial melts in regions below mid-ocean ridges, regions above and below the mantle-transition region, and atop the core-mantle boundary. These hydrous silicate magmas are thus important in controlling the storage and transport of water in the interior[3].

Hydrogen dissolved in silicate melts can significantly influence the host physical properties, for instance, by lowering the density and enhancing the electrical conductivity[4-9]. One of the major goals is to constrain the partial molar volume of water in silicate melts as a function of pressure, temperature, and composition[6,7,10,11]. This is important in evaluating the density of melts for different water contents at the relevant conditions of the Earth's interior. It is the density of silicate melts relative to the density of the surrounding mantle rocks that determines the direction and rate of melt migration and the amount of melt when partial melting occurs at a depth[12,13]. The melt-crystal density crossover may have played a crucial role in the processes that governed the fractional crystallization and chemical differentiation of early magma oceans as well as in the large fraction of geological history[3,14,15]. Like the density, the electrical conductivity of silicate melts can be compared with magnetotelluric survey data to detect and quantify possible partial melts in the mantle[16-18].

A large number of experimental data is available for hydrous silicate melts at upper mantle-transition zone conditions[19]. For instance, the measured data at pressures up to 20 GPa in the temperature range 1273 to 2473 K have recenlty been used to derive the equation of state for the partial molar volume of water ($\bar{V}_{\mathrm{H_2O}}$) in magmas[10]. While an overall decreasing trend of $\bar{V}_{\mathrm{H_2O}}$ with pressure is evident, the extent of pressure-induced variations among different measurements and different melt compositions is large and some data even show anomalous increase with compression[10,20,21]. The measured electrical conductivity data for hydrous silicate melts, are rather scarce and scattered[8,9,22,23]. One primary reason for such inconsistency and difficulty could be associated with the difficulty of quantifying the water content of the samples due to water loss during high temperature experiments.

On the other hand, a relatively few computational studies of hydrous silicate melts have so far been reported using first-principles approach[6,7,24-26]. These studies have covered relatively high temperatures and chemically simple compositions. Moreover, these computations may have been biased in a quantitative sense. For example, the use of the local density approximiation (LDA) for the exchange-correlation functional tends to overbind the structure leading to significant underestimation of the volume[6]. While the calculated partial molar volume of water appears to be mostly insensitive to water concentration[26] and melt composition[6,24,25], the issue is yet to be fully resolved. Similarly, it is not clear how hydrous contributions to electrical conduction are sensitive to pressure, temperature, and composition.

Here, we evaluate the partial molar volume ($\bar{V}_{H_2O}$), speciation, and diffusion coefficients (and the contributions to electrical conductivity) of the water component by performing first-principles molecular dynamics (FPMD) simulations of hydrous $Mg_{1-x}Fe_xSiO_3$ and $Mg_{2(1-x)}Fe_{2x}SiO_4$ liquids for $x = 0$ and 0.25 within the generalized gradients approximation (GGA) as in our recent study[25]. These melt systems differ in the degree of structural polymerization with ($Mg_{1-x}$ + $Fe_x$) / Si ratio of 1 and 2. We consider three different concentrations of water (6.0, 8.2, and 11.4 wt%) and wide ranges of pressure (0 to 140 GPa) and temperature (2000 to 4000 K). We can use the calculated properties of bulk (pure) liquid water as a basis to ascertaining the effects of water on melt properties. For instance, molar volume of water, $V_{H_2O}$, may be taken as an upper bound on $\bar{V}_{H_2O}$. The high-pressure behavior of water is also crucial to our understanding of giant planets[27,28] and shock wave data[29]. The pressure and temperature space considered here covers the phase transition of water from a molecular liquid to a dissociated liquid[30]. Finally, we use the simulated results to model the effects of water on the density and electrical conductivity of silicate melts and discuss their geophysical implications.

## Results and Analysis

*Equation of State of Hydrous Silicate Melts and Pure Water*

We present the calculated pressure-volume-temperature (*P*-*V*-*T*) results for all hydrous and dry $Mg_{1-x}Fe_xSiO_3$ and $Mg_{2(1-x)}Fe_{2x}SiO_4$ melts for $x = 0$ and 0.25 in Fig. 1. The volume of hydrous melts is systematically larger than the volume of the corresponding water-free melts for the supercells used. Our simulations cover the pressure ranges 0 to ~30 GPa at 2000 K, 0 to ~115 GPa at 3000 K, and ~35 to ~140 GPa at 4000 K. In the overlapping pressure regimes, the volume at a higher temperature is larger than the volume at a lower temperature. The calculated results can be adequately represented using the following relation[7,13]

$$P(V,T) = P(V,T_0) + B_{TH}(V)(T-T_0) \quad (1)$$

Here the reference isotherm, $P(V,T_0)$ with $T_0$ = 3000 K, is described by the 4th order Birch-Murnaghan equation with fit parameters shown in Table 1. Hydrous melts have relatively small zero-pressure bulk moduli, meaning that they are highly compressible at low pressures. The pressure-volume isotherms become nearly parallel with those of dry melts at high pressure. The thermal pressure coefficient in Eq. 1 is expressed by

$$B_{TH}(V) = \frac{1}{1000}\left[a + b\left(\frac{V_0}{V}\right) + c\left(\frac{V_0}{V}\right)^2 + d\left(\frac{V_0}{V}\right)^3\right] \quad (2)$$

where $V_0$ is the volume at zero pressure and 3000 K (Table 1). Our calculated *P*-*V*-*T* results can be also described by an alternative form for the equation of state, which is based on the hard-sphere model[31] (Supplementary Text 1). While two forms of equation of state agree well within the interpolation pressure regime at a given temperature, they tend to differ considerably at extrapolated pressures (Supplementary Fig. S1)

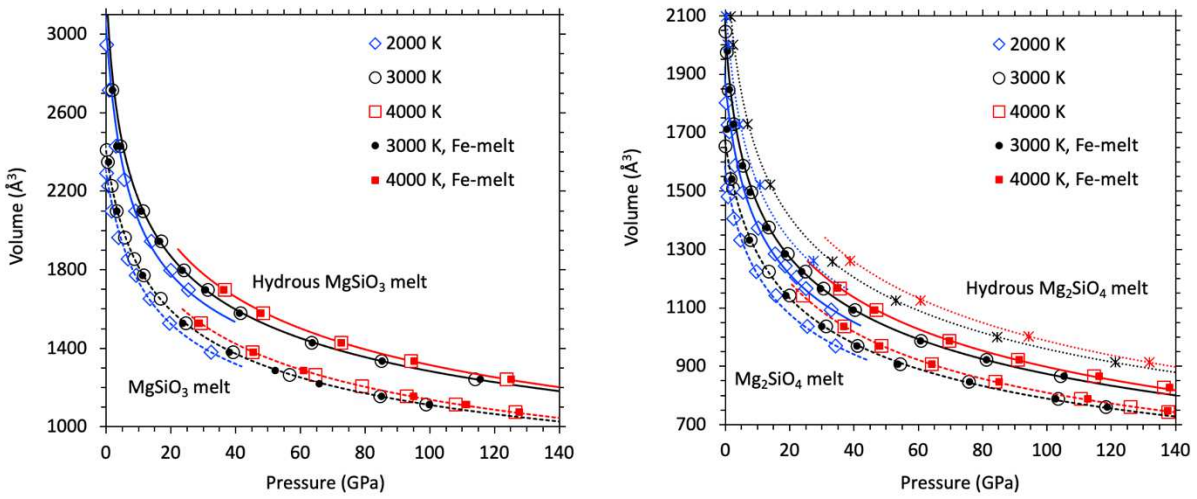


**Figure 1.** The volume-pressure profiles of hydrous $MgSiO_3$ (left) and $Mg_2SiO_4$ (right) melts compared to their dry counterparts at 2000 K (blue diamonds), 3000 K (black circles) and 4000 K (red squares). Curves represent the equation of state fits using Eq. 1 and 2. The supercells consist of $32MgSiO_3$+$16H_2O$ (8.2 wt% water) and $16Mg_2SiO_4$+$8H_2O$ (6.0 wt% water) and corresponding iron-bearing phases at 3000 and 4000 K (small solid symbols). Also shown are the results for $16Mg_2SiO_4$+$16H_2O$ (11.4 wt% water) at three temperatures (asterisks and dotted curves).

**Table 1.** Equation of state parameters of hydrous and dry silicate melts at 3000 K.

| | Hydrous $MgSiO_3$ | Dry $MgSiO_3$ | Hydrous $Mg_2SiO_4$ | Dry $Mg_2SiO_4$ |
|---|---|---|---|---|
| $V_0$(Å$^3$) | 3280 | 2415 | 2050 | 1670 |
| $\rho_0$ (g/cm$^3$) | 1.772 | 2.209 | 1.940 | 2.238 |
| $K_0$ (GPa) | 8.2 | 19.1 | 11.3 | 22.2 |
| $K_0'$ | 4.85 | 4.02 | 5.53 | 3.94 |
| $K_0''$(GPa$^{-1}$) | -0.50 | -0.08 | -0.69 | -0.06 |
| *a* | 26.9 | 32.7 | 19.9 | 7.9 |
| *b* | -53.8 | -70.9 | -41.6 | -23.4 |
| *c* | 34.0 | 49.3 | 28.2 | 21.1 |
| *d* | -6.1 | -9.9 | -5.2 | -4.5 |

We represent the pressure-volume-temperature results of pure water (Fig. 2) with Eq. 1 with the addition of a constant pressure term ($P_0$ = 0.5 GPa) for the reference 2000 K isotherm (Table 2). The volume-dependent thermal pressure coefficient is given by $B_{TH}(V) = -0.92 + 1.2\left(\frac{V_0}{V}\right) + 0.07\left(\frac{V_0}{V}\right)^2$ in the units of mPa/K, where $V_0$ is volume at $P_0$. Pure water is highly compressible as

reflected by its unusually small bulk modulus. For instance, the volume along the 2000 K isotherm decreases from 39 $cm^3mol^{-1}$ at 0.5 GPa to 16 $cm^3mol^{-1}$ at 5 GPa. It changes more gradually as the fluid is compressed further. Different isotherms tend to become parallel and remain close to each other at high pressures. The calculated volume remains above 5.5 $cm^3mol^{-1}$ at 150 GPa. Our pressure-volume results at 1000 and 2000 K are similar to the previous calculations which used GGA and relatively large supercells[32]. The experimentally inferred data on liquid water are confined to low pressures and low temperatures[33-35]. Our comparisons with the experimental data indicate that GGA overestimates the volume (lying within 5%) whereas LDA underestimates the volume (differing by up to 15%) as shown in Fig. 2. A similar degree of volume overestimation and hence density underestimation by GGA was previously predicted[32] for the 300 K isotherm of ice VII/X compared to the measured data over much wider pressure range up to 126 GPa[29,36].

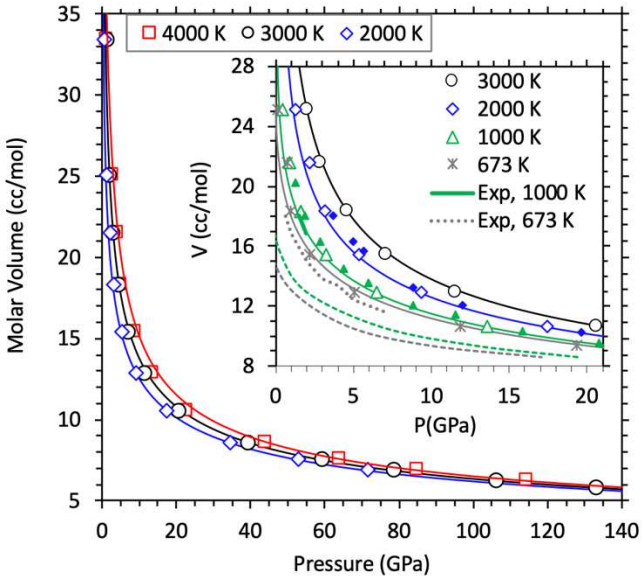


**Figure 2.** Volume-pressure relationships of pure liquid water at 2000, 3000 and 4000 K. Symbols represent the calculated values and curves represent the corresponding equation of state fits. The inset compares our calculated results (symbols and curves) with the available low-pressure experimental data at 673 and 973 K[34,35] and the previous calculations shown by small solid triangles and diamonds[32]. Also shown are the LDA results at 673 and 1000 K (green and gray dashed lines) which are shifted downward with respect to both the GGA and experimental results.

*Partial Molar Volume of Dissolved Water*

We evaluate the partial molar volume of water in silicate melt ($\bar{V}_{H_2O}$) from the direct volume difference between hydrous ($V_{hymelt}$) and dry ($V_{melt}$) melts:

$$\bar{V}_{H_2O}(P,T) = \left(V_{hymelt}(P,T) - V_{melt}(P,T)\right)N_A/n \qquad (3)$$

where $n$ is the number of $H_2O$ units in the supercell and $N_A$ is Avogadro's number. Fig. 3 shows the calculated partial molar volume of water in hydrous $MgSiO_3$ and $Mg_2SiO_4$ melts and in their iron-bearing phases. We model the compression behavior of $\bar{V}_{H_2O}$ using Eq. 1. The reference isotherm $P(V,T_0)$ with $T_0$ = 2000 K considering all results for three iron-free melts (Fig 3, left) is described by the 4th order Birch-Murnaghan equation of state (Table 2). The zero-pressure bulk modulus is small, consistent with experimentally inferred value[10]. The thermal pressure coefficient in the 2000 to 4000 K range can be described by $B_{TH}(V) = 0.3 - 0.8\left(\frac{V_0}{V}\right) + 0.9\left(\frac{V_0}{V}\right)^2$ in the units of mPa/K. For each hydrous silicate melt, $\bar{V}_{H_2O}$ decreases rapidly initially with increasing pressure and then decreases more gradually at higher pressures. Hydrous enstatite melts tend to have larger $\bar{V}_{H_2O}$ than hydrous forsterite melts at pressures close to zero, but they have similar values over much of the pressure regime explored. It is also remarkable that the iron-induced differences in $\bar{V}_{H_2O}$ are negligible at all conditions (Fig. 3, right). Our results thus suggest that the partial molar volume of water remains insensitive to melt composition within the computational uncertainty over almost entire mantle pressure regime (except at low pressures up to 5 GPa).

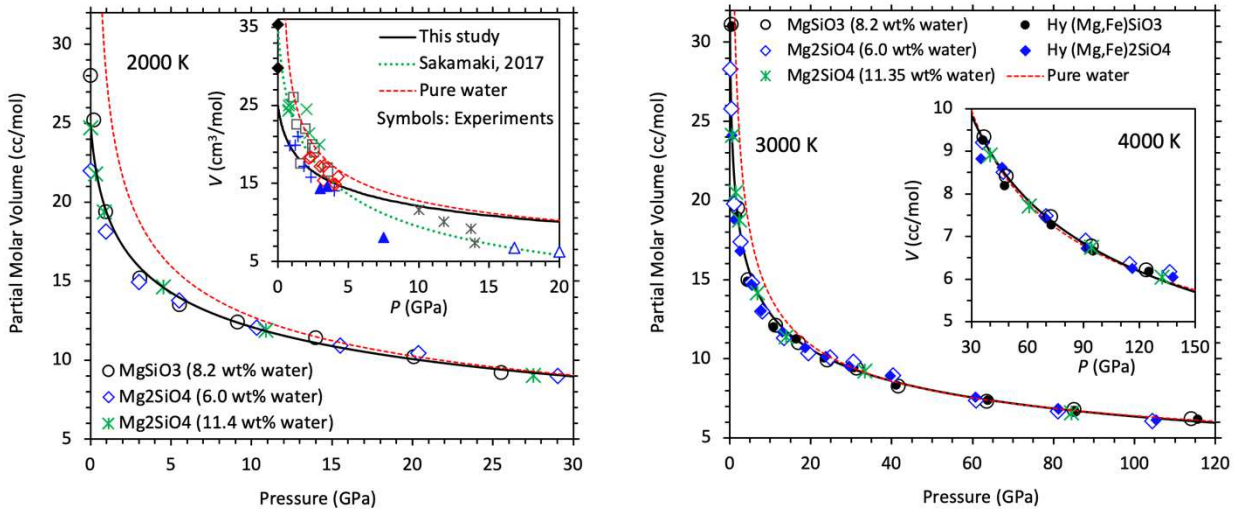


**Figure 3.** Calculated partial molar volume of water in hydrous $MgSiO_3$ enstatite melt (8.2 wt% water) and $Mg_2SiO_4$ forsterite melts (6.0 and 11.4 wt% water) at 2000 K and in their iron-free and iron-bearing phases ($Mg_{1-x}Fe_xSiO_3$ and $Mg_{2(1-x)}Fe_{2x}SiO_4$ for $x$ = 0 and 0.25) at 3000 and 4000 K as a function of pressure. Also shown is the equation of state fit to all melt results together at each temperature (solid curve) compared to the calculated equation of state for pure water (red dashed curve). The inset on left shows the experimental data on the partial molar volume of water in several silicate melts in the temperature range 1273 to 2473 K projected to 2000 K using the model of Sakamaki[10]. Different symbols represent different melt compositions, plus: andesite[39], solid triangle: basalt[12], square: granite[40], open triangle: komotiite[41], open diamond: peridotite[5], cross: phonolite[42], and asterisk: ultramafic[4,31]; solid diamond: hydrous silicate melts at 0 GPa[20,21].

**Table 2.** Equation of state parameters at 2000 K for the dissolved water by considering together the results for all hydrous iron-free melts ($MgSiO_3$ with 8.2 wt% water, $Mg_2SiO_4$ with 6.0 and 11.4 wt% water). The experimentally inferred parameters are from Sakamaki[10]. The parameters for pure liquid water correspond to a non-zero constant pressure (0.5 GPa).

| | Water in silicate melts | | Pure Water |
|---|---|---|---|
| | Calc | Expt | Calc |
| $T_0$(K) | 2000 | 2000 (1273) | 2000 |
| $V_0$(cm$^3$/mol) | 25.0 | 35.5 (23.8) | 39.0 |
| $K_0$ (GPa) | 1.91 | 1.23 (1.18) | 0.72 |
| $K_0'$ | 5.80 | 3.31 (3.35) | 4.13 |
| $K_0''$(GPa$^{-1}$) | -5.1 | -2.81 (-2.95) | -5.2 |

We compare the calculated $\bar{V}_{H_2O}$ of hydrous melts at 2000 K with the experimental data in the temperature range 1273 to 2473 K at pressures up to 20 GPa in the inset of Fig. 3, left. The experimental melt compositions are more complex, including albite[37,38], andesite[39], basalt[12], granite[40], komotiite[41], peridotite[5], phonolite[42], rhyolite[20], and ultramafic[4,31]. The reported values at the ambient pressure and 1273 K for $\bar{V}_{H_2O}$ and its temperature derivative ($\partial\bar{V}_{H_2O}/\partial T$) are 22.9 cm$^3$mol$^{-1}$ and 9.5 $\times 10^{-3}$ cm$^3$mol$^{-1}$K$^{-1}$, respectively[20]. More recently reported values[21] are 23.8 cm$^3$mol$^{-1}$ and 15.9 $\times 10^{-3}$ cm$^3$mol$^{-1}$K$^{-1}$. These studies have suggested that the partial molar volume of water is independent of the melt composition and water concentration. Using these two sets of the parameters, we estimate $\bar{V}_{H_2O}$ to be 29.8 and 35.4 cm$^3$mol$^{-1}$ at 2000 K and 0 GPa. They are larger than our predicted values of 28.0 cm$^3$mol$^{-1}$ for hydrous enstatite melt and 23.5 cm$^3$mol$^{-1}$ for hydrous forsterite melt.

Comparison of the calculated partial molar volume of water in silicate melts ($\bar{V}_{H_2O}$) with the molar volume of pure liquid water ($V_{H_2O}$) allows us to assess the nature of mixing between the volatile and silicate components. As shown in Fig. 3, $\bar{V}_{H_2O}$ is smaller than $V_{H_2O}$ at zero pressure but the two volumes approach each other rapidly with increasing pressure. The volume of the melt + water solution is large negative (-18.8 cm$^3$mol$^{-1}$ at 0.5 GPa and 2000 K) and remains negative at pressures below 15 GPa, but it becomes zero with further compression. This means that its behavior changes from non-ideal to ideal with increasing pressure. Non-ideal mixing of silicate melts and $H_2O$ fluid was also implied experimentally at low pressures[43-45].

*Hydrogen and Oxygen Diffusion*

We find that hydrogen is highly mobile in all melts simulated in general agreement with previous computational results[26,46,47]. At each temperature, the diffusivity decreases with

increasing pressure implying positive activation volume and all log$D_H$-$P$ isotherms tend to be linear (Fig. 4). Comparison of these isotherms among different melts suggests that hydrogen diffuses somewhat faster in hydrous silicate melts with higher water content (Supplementary Fig. S2). The presence of iron tends to enhance hydrogen diffusion and diminish the differences in $D_H$ between the two silicate melt systems (Supplementary Fig. S2). Oxygen diffuses much slower than hydrogen (Fig 4). At 2000 K, the $D_H/D_O$ ratio increases from ~4 to more than 10 over the pressure range 0 to 30 GPa. At 3000 K, this ratio exceeds 10 above 50 GPa and becomes so large at 80 GPa that O atoms (as well as Mg and Si atoms) can essentially be assumed as frozen with respect to H. At 4000 K, all atomic species including oxygen diffuse at discernable rates even at very high pressures. Our results thus suggest that hydrogen diffuses a few orders of magnitude faster than the host ions in silicate melts even at the conditions applicable to the deepest parts of the mantle.

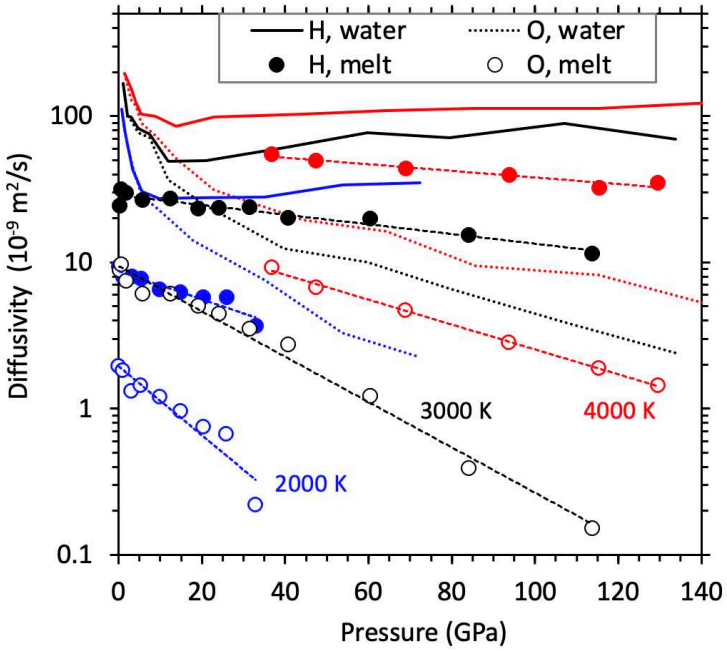


**Figure 4.** Diffusivity-pressure profiles of hydrogen and oxygen of hydrous silicate melts (symbols) taken as averages over five melt compositions at 2000 K (blue), 3000 K (black), and 4000 K (red). Their Arrhenius trends are represented by straight dashed lines. Also shown are the diffusivity results of pure water (solid curves for H and dotted curves for O).

In pure liquid water, hydrogen and oxygen diffuse in a different manner than in silicate melts. As pressure increases, both diffusivities ($D_H$ and $D_O$) decrease rapidly almost overlapping with each other in low-pressure regime (Fig. 4), that is, the $D_H/D_O$ ratio remains close to 1 implying the diffusion of individual $H_2O$ molecules. The simulated water is thus considered to be a molecular fluid at low pressures irrespective of temperature. As pressure increases beyond ~10 GPa, hydrogen and oxygen diffusion decouple from each other. The $D_H$ profile reaches shallow minimum before it shows a gradual increasing trend at high pressures. On the other hand, the

oxygen diffusivity continues to decrease with increasing pressure. The two diffusivity profiles systematically diverge with compression, for instance, the $D_H/D_O$ ratio is ~16 at 72 GPa (2000 K) and 24 at 142 GPa (4000 K). Because hydrogen diffuses much faster than oxygen, the simulated water essentially represents a dissociated fluid state over much of the pressure regime studied.

We find that the calculated hydrogen and oxygen diffusivities of hydrous silicate melts are much smaller than those of the bulk water particularly at low temperatures (Fig. 4). Also, melt $D_H$ and $D_O$ differ from each other at all pressures, including zero pressure. Melt $D_H$ decreases gradually with pressure with no anomalous behavior shown by water $D_H$. Melt $D_O$ decreases monotonically with pressure though more rapidly than water $D_O$. In silicate melt, oxygen diffusion is also controlled by Mg-O and Si-O bond events. Our results show that the diffusivity isotherms of hydrous silicate melts and pure water differ more as pressure increases.

*Speciation of Hydrous Component and Structure of Water*

Hydrogen exclusively forms bond with oxygen in hydrous silicate melts as in bulk water. This is reflected by a sharp peak around 1 Å in the H-O radial distribution function and a broad peak in all other hydrogen-involved functions (Supplementary Fig. S3 and S4). So, the speciation of hydrous component in melts is determined by the local coordination environments of H and O. The calculated mean H-O coordination number ($Z_{HO}$) of hydrous silicate melts is slightly larger than 1 at zero pressure and its value increases almost linearly with pressure along each isotherm (Fig. 5, left). Melt $Z_{HO}$ always remains above water $Z_{HO}$ (which is 1 at zero pressure) with larger differences between them appearing at higher pressures. At zero pressure, we find that a small proportion (2-3%) of hydrogen atoms are coordinated with two oxygen atoms (that is, forming -O-H-O- bridge) in melts whereas all hydrogen atoms are singly oxygen-coordinated in water. The proportion of two-fold and one-fold coordination states increases and decreases, respectively, with increasing pressure more rapidly in melts compared to water (Supplementary Fig. S5). In the case of iron-bearing silicate melts, hydrogen has an affinity for iron, which is manifested by shoulder-like feature in the H-Fe radial distribution function (Supplementary Fig. S3). The associated H-Fe bonding tends to cause a slight reduction in $Z_{HO}$.

On the other hand, the O-H coordination environment is sensitive to the Mg/Si ratio of melts. The calculated mean O-H coordination number ($Z_{OH}$) at zero pressure is 0.29 for hydrous $MgSiO_3$ melt and 0.23 for hydrous $Mg_2SiO_4$ melt. Its value increases with increasing pressure for both melts, and the differences between two melts persist at all pressures (Fig. 5, right). As expected, a large fraction of oxygen (~80%) is not bonded with hydrogen in melts. The rest of oxygen form mostly hydroxyls and some molecular water at low pressure (Fig. 6), generally consistent with the experimental observations[48,49]. In contrast, every oxygen is bonded with two hydrogen atoms in water corresponding to $Z_{OH} = 2$ (and $Z_{HO} = 1$) and nearly 100% $H_2O$ molecules at zero pressure (Fig. 6). On compression, oxygen is increasingly bonded with hydrogen in water and $Z_{OH}$ exceeds 3 at high pressures. The proportion of $H_2O$ molecules in water decreases rapidly as pressure increases (Supplementary Fig. S5), dropping to ~85% at 20 GPa, then to ~50% at 50 GPa and

~10% above 100 GPa. Larger groups, such as $OH_3$, $OH_4$ and $OH_5$ all become increasingly abundant at higher pressure (Supplementary Fig. S5). Moreover, they are linked with each other to form more complex species as hydrogen is shared with two or even three oxygens. A clear structural change thus occurs from a molecular liquid to a dissociated liquid (with larger $OH_n$ groups and probably more ionic in nature) as the liquid water is compressed (Fig. 6). Two oxygen coordinated states of hydrogen (that is, -O-H-O-) facilitate hydrogen movement in both water and hydrous silicate melts.

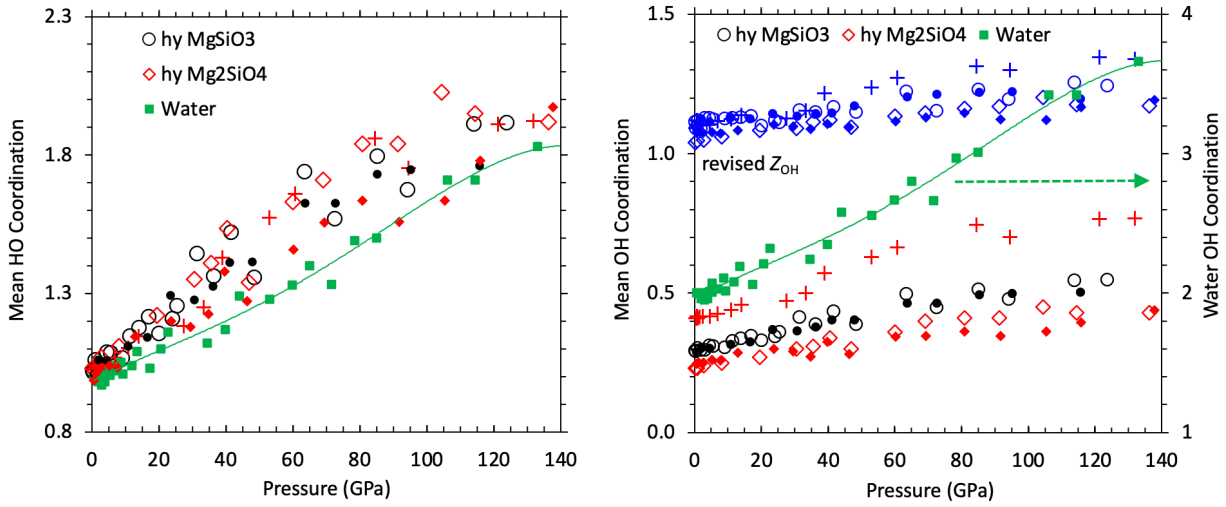


**Figure 5**. Mean H-O and O-H coordination numbers of hydrous $MgSiO_3$ with 8.2 wt% water (circles) and $Mg_2SiO_4$ with 6.0 wt% water (diamonds) and 11.4 wt% water (pluses) compared to those of water (solid squares). The revised $Z_{OH}$ (right) represents the mean coordination number evaluated by considering only oxygen atoms that contribute to the coordination. The results for the corresponding iron-bearing phases are shown by small solid symbols.

Pressure systematically enhances oxygen-hydrogen bonding in hydrous silicate melts. Considering only oxygen atoms which are bonded with hydrogen, the revised value of $Z_{OH}$ increases from ~1.1 to ~1.25 for hydrous $MgSiO_3$ melt and from ~1.05 to ~1.20 for hydrous $Mg_2SiO_4$ melt over the pressure ranges considered here (Fig. 5, right). The majority of oxygen (80 to 95%) are singly coordinated with hydrogen in silicate melts. The proportion of singly and doubly hydrogen-coordinated species (that is, hydroxyls and $OH_2$) gradually decreases and increases, respectively, with increasing pressure (Supplementary Fig. S5). Even hydronium group ($OH_3$) appears in discernable amounts (up to ~3%) above 30 GPa. This pressure enhancement of two-fold coordination states comprising of hydrogen and oxygen (that is, -O-H-O- and -H-O-H- groups) in silicate melts indicates a changing role of hydrogen from a network modifier at low pressure to a network former at high pressure (Fig. 6). The predicted pressure evolution of the hydrous speciation is generally consistent with previous computational studies of hydrous silicate melts[6,7,24-26].

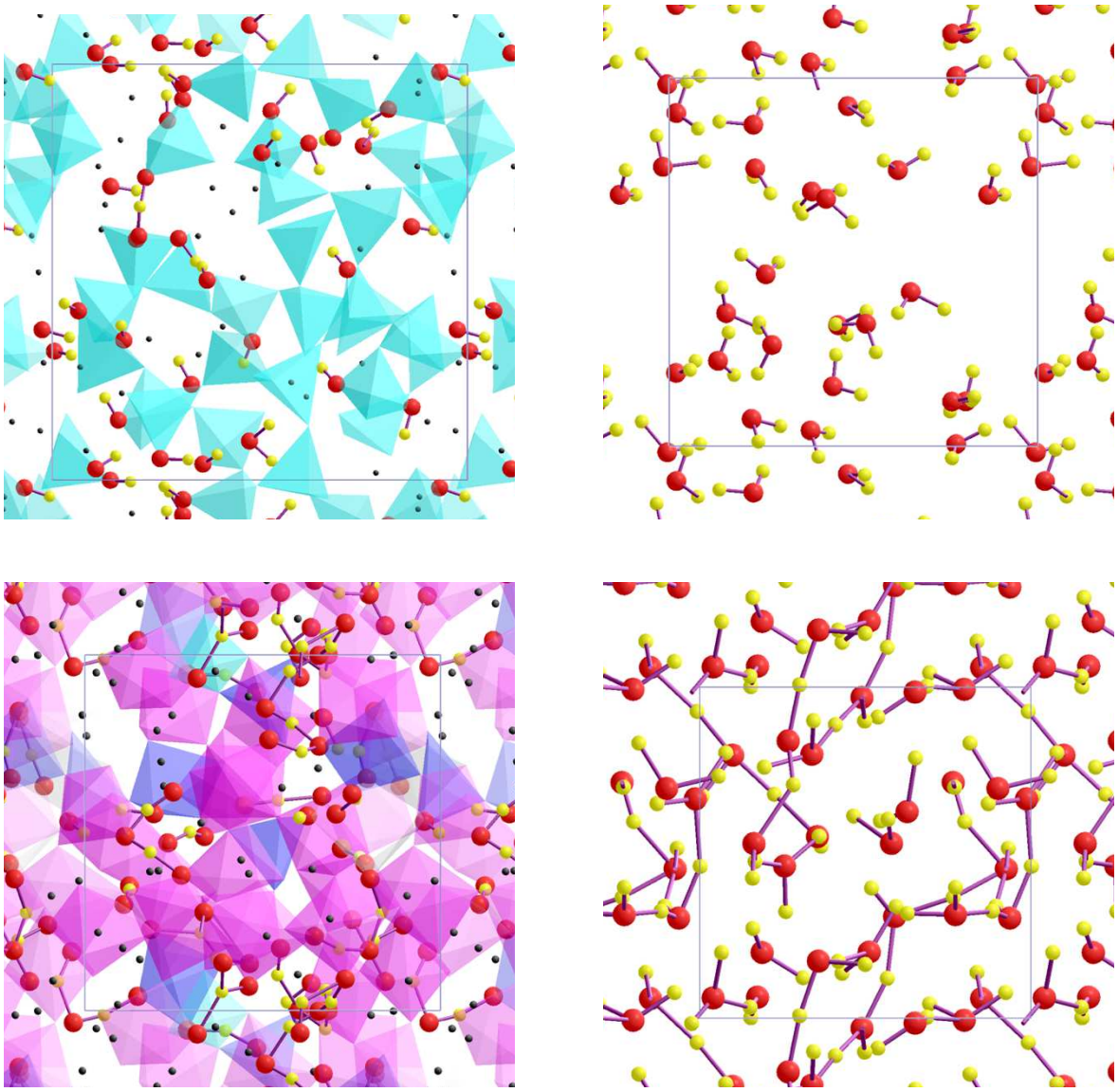

**Figure 6**. Visualization snapshots of hydrous silicate melt (32 $MgSiO_3$ + 16 $H_2O$) and bulk water (24 $H_2O$) at low and high pressures[59]. The hydrous melt consists of mostly hydroxyls with one $H_2O$ molecule and one -O-H-O- bridge at 0.2 GPa and 2000 K (top-left). It shows fewer hydroxyls, many -O-H-O- bridges, and longer sequences (-O-H-O-H-O-, -O-H-O-H-O-H-O-, $HO_3$) at 85.1 GPa and 3000 K (bottom-left). Also shown are the Si-O coordination states (cyan: tetrahedron, blue: pentahedron, magenta: octahedron) and Mg atoms (black dots). The simulated pure water contains only water molecules at 0.7 GPa and 2000 K (top-right). A highly compressed water (79.4 GPa and 3000 K) contains ten $OH_2$, twelve $OH_3$, and two $OH_4$, which are also interconnected with each other via hydrogen (bottom-right).

## Discussion and Implications

*Melt+water solution.* The predicted negative volume of silicate melt+water solution at low pressures (for instance, -19, -2.7, and -0.7 $cm^3mol^{-1}$, respectively, at 0.5, 5, and 10 GPa at 2000 K) can be attributed to the differences in local hydrogen-oxygen arrangement between silicate melt and pure water. The water component is dissolved in silicate melts primarily as hydroxyls and to some extent as molecular water, which are also bound to one or more cations via oxygen bonding (Fig. 6, left)). This means that the incorporation mechanism is predominantly chemical. On the other hand, the bulk water is in molecular liquid state exclusively consisting of loosely (physically) bound $H_2O$ molecules at low pressures (Fig. 6, top-right)). Such a molecular fluid water is highly compressible, so its volume becomes comparable to the partial molar volume of the dissolved water in the melt at pressures above 15 GPa (Fig. 3). The pressure-induced similarity between two volumes can be associated with our finding that the $H_2O$ component in melts as well as the bulk water become structurally well-connected (that is, exclusively chemical) at high compression. Enhanced participation of oxygen in hydrogen bonding becomes notable and also the proportions of species, such as $H_3O$ and $H_4O$, are large in highly compressed bulk water, which represents the dissociation of water as in the case of hydrous melts. The mixed system thus becomes increasingly ideal on compression. This explains the experimental observations suggesting that water and silicate melt become completely miscible at high pressures[45]. Our finding that hydrous melts of different compositions (varying Mg/Si and iron content) behave similarly at all pressures suggests that the predicted effects of hydration on melt properties are likely to be applicable to natural melt compositions as well.

Most previous first-principles computations used LDA to study silicate melts, including hydrous ones[6,7,46,47]. Comparison of our new results with the previous results allow us to assess how much the evaluation of partial molar volume is sensitive to the choice of the exchange correlation functional. A general trend is that GGA gives systematically larger volume than LDA. This is indeed the case with both pure and hydrous silicate melts. The volume difference between GGA and LDA for these melts is large at zero pressure (~15%) and it decreases gradually with increasing pressure (~5% at 50 GPa). This trend is also evident in the bulk water for which the volume difference is very large particularly at low pressures (~50% at 0.5 GPa, ~20% at 5 GPa), dropping below 5% at pressures beyond 100 GPa. In the case of the partial molar volume of water, the GGA-LDA difference is large at low pressures but it vanishes within our computational uncertainty at high pressures.

*Density change by hydration.* The water-induced reduction in the melt density tends to be nearly uniform with respect to pressure and temperature[6,7,24]. The calculated density contrasts (Fig. 7) can be adequately described with the following relation:

$$\frac{\rho-\rho_0}{\rho_0} = (-0.56 + 0.057\ln(P))(x_{\mathrm{m}}/100) \qquad (4)$$

where $\rho$ is the density of hydrous silicate melt, $\rho_0$ is the density of non-volatile component (dry silicate melt), and $x_m$ is the mol percent of water in terms of oxide components. The reduction in melt density by hydration thus depends linearly on water concentration. The density contrast varies gradually with pressure according to Eq. 4 (over much of the pressure regime except below 5 GPa), which is independent of temperature and melt composition within the computational uncertainty (Fig. 7). Our model differs from the previous model[24] which assumed that the density contrast only depends on water content in terms of weight percent. We find that the amount of water in terms of mol percent determines the magnitude of density contrast more accurately than that in terms of weight percent. This perhaps makes sense because the density changes are related to the dilation caused by the hydrous component. If the melt+water solution is strictly ideal at all conditions, the density contrast between hydrous and anhydrous melts will vary rapidly initially and then gradually with pressure. The predicted hydration density at low pressures is smaller than that in an ideal mixing case.

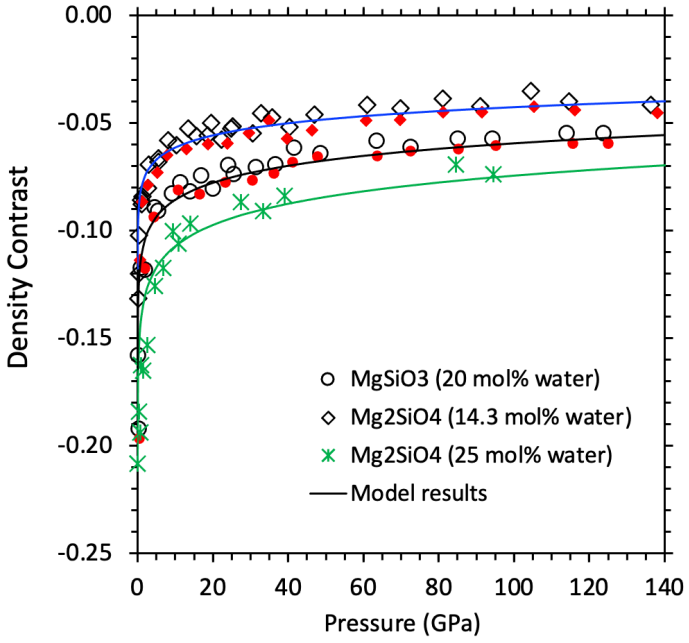


**Figure 7**. Density contrast between dry and hydrous melts for iron-free (open symbols and asterisks) and iron-bearing (filled small symbols) compositions as a function of pressure. The model results using Eq. 4 are shown by curves.

Silicate melts were prevalent in magma ocean environment soon after Earth was formed. Now they are present to much smaller extents, most likely in regions below mid-ocean ridges, regions above and below the mantle-transition region, and atop the core-mantle boundary. A melt formed just above the mantle transition zone can be gravitationally stable if the melt density takes a value

between the density of the upper mantle minerals near 410 km depth (3.54 g/cm$^3$) and the density of the materials at the top of mantle transition zone (3.73 g/cm$^3$). Using Eq. 4 with a density contrast evaluated[50] as (3.54 - 3.73)/3.73 = -0.051, we obtain $x_m$ = 12.4 mol% at 14 GPa. This means that a melt containing up to 5 wt% water will be stable atop the mantle transition zone if the FeO content of melt is 0.25. Similarly, we estimate that up to 9 wt% water may be accommodated in a buoyantly neutral hydrous melt at the 660 km depth discontinuity corresponding to its large density jump[50] of 0.38 g/cm$^3$. The implied presence of gravitationally trapped at hydrous partial melts at these depths have been previously suggested[6,12,26,51]. The water content of possible melts at these depths also depends on the iron content as water and iron change the density in an opposite way. Both iron and water are preferably partitioned into melts when partial melting occurs at a depth or when a magma ocean starts to crystallize resulting in a dense hydrous melt.

*Electrical conductivity.* Highly mobile hydrogen ions carrying positive charges (as protons) can contribute to the electrical conductivity ($\sigma$) of melts. We evaluate this contribution from the calculated diffusivity ($D$) values (Fig. 4) using the Nernst-Einstein relation as previously done[7]

$$\sigma = \frac{Dnq^2}{kTH_R} \qquad (5)$$

where $n$ is the number density of mobile carriers with electrical charge $q$, and $k$ denotes the Boltzmann constant. The Haven ratio $H_R$ is a correlation factor for the ionic motion and approaches one for small $n$, so we take $H_R$ = 1. For hydrous silicate melts, we consider protons ($H^+$ ions) as the primary charge carriers; $q$ = +1e. Our results show that the hydrogen-induced (ionic) conductivity of hydrous silicate melts ($\sigma_{melt}$) takes larger value at higher temperature, but along each isotherm it remains almost constant with respect to pressure (Fig. 8; Supplementary Fig. S6). The average conductivity over the pressure ranges considered here corresponds to 100, 247, and 480 S/m, respectively, at 2000, 3000, and 4000 K for (Mg,Fe)$SiO_3$ melts with 20.0 mol% water. The corresponding $\sigma_{melt}$ values of hydrous $(Mg,Fe)_2SiO_4$ melts are 63, 160, and 293 S/m for 14.3 mol% water and 138, 328, and 597 S/m for 25.0 mol% water. As expected, hydrous melt becomes more conductive for higher water concentration. These average conductivity values can be described by the following concentration-dependent Arrhenius model:

$$\sigma(x_m, T) = \sigma_0 \exp[-E/(RT)] \qquad (6)$$

where $\sigma_0(x_m) = -435 + 12150\, x_m$ is the pre-exponential factor, varying linearly with the mol percent of water ($x_m$), and $E$ = 50±2 kJ/mol is the activation energy which is independent of water content. The model predicts a value of 43 S/m at 1873 K and 14 GPa, which compares well with the experimentally inferred value[8] of 37 S/m.

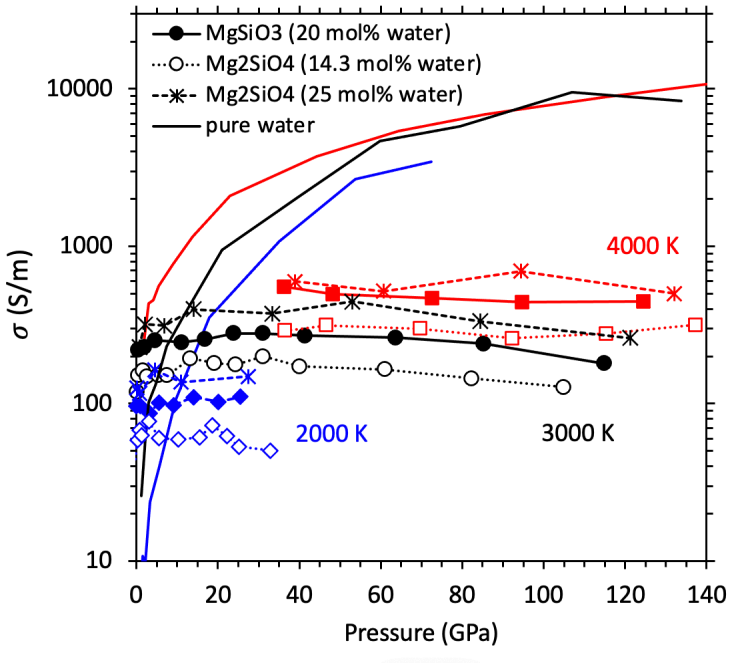


**Figure 8.** Hydrogen-induced electrical conductivity ($\sigma$) of hydrous $MgSiO_3$ (filled symbols) and $Mg_2SiO_4$ melts (open symbols and asterisks) and bulk water (solid curves) as a function of pressure at different temperatures. The melt conductivity at 3000 and 4000 K represent the averages taken between the iron-free and iron-bearing compositions (iron has almost no influence on the conductivity).

In pure water, hydrogen diffuses primarily as neutral $H_2O$ molecules at low pressure. We exclude the hydrogen atoms of molecular water by approximating the effective concentration of charge carriers by $(1\text{-}f)n$, where $f$ is the proportion of $H_2O$ species. The estimated electrical conductivity of bulk water ($\sigma_{water}$) increases rapidly initially and then gradually as pressure increases (Fig. 8). Our results compare favorably with previous computational results[30,52]. and measured shock wave data[53,54]. The predicted pressure behavior represents ionic conduction as water upon compression changes from an insulating molecular liquid to a fully dissociated ionic liquid. Highly compressed water behaves as a superionic liquid in which oxygen ions essentially become frozen compared to highly mobile hydrogen ions ($D_O$ is one to two orders of magnitude smaller than $D_H$ as shown in Fig. 4). We find that $\sigma_{water}$ is smaller than $\sigma_{melt}$ at pressures up to 10 GPa when pure water behaves as a molecular fluid (Fig. 8). As the water is compressed further, $\sigma_{water}$ exceeds $\sigma_{melt}$ because hydrogen ion diffuses via O-H bond breaking/formation events. Both the concentration and diffusion rate of charge carriers ($H^+$) in compressed bulk water are high compared to those in hydrous silicate melts.

We estimate the electrical conductivity of a gravitationally stable partial melt layer at 410 km depth containing 5 wt% water as discussed above. This corresponds to $x_m \sim 13$ mol% for which using Eq. 6 gives $\sigma_{melt}$= 39 S/m at 1800 K. So, a partial melt containing a few percent (say, 3

volume %) of hydrous melt corresponds to a high conductivity of ~1.3 S/m. Electrical conductivities in the range 0.1 to 2.0 S/m have been reported in the upper-mantle-transition regions by electromagnetic sounding observations[16-18].

*Summary.* In most cases, silicate melts contain some water. Whether such hydrous melt sinks or rises or stagnates at a depth controls the amount of water that may be entertained in the interior and its subsequent contributions to global water cycle at all times of Earth's history. For instance, upwelling hydrous magmas may have been contributing to the origin and maintenance of the atmosphere and hydrosphere. To better understand these issues requires a full knowledge about the behavior and properties of hydrous silicate melts at relevant pressure and temperature conditions. This study represents a major step in this endeavor as it reports the results of first-principles molecular dynamics simulations of hydrous silicate melts covering wide ranges of pressure (up to 140 GPa), temperature (2000 to 4000 K), and composition (water content, Mg/Si ratio, iron content). Using the simulation results, we have made quantitative evaluation of the effects of water on the density and electrical conductivity of silicate melts. These effects are further linked to the thermodynamic and structural differences between water in silicate melts and water in its bulk (pure) form. The water component is much more compressible than bulk water, particularly at low pressures. Water is dissolved in melts in dissociated form mostly as hydroxyls at low pressure and as extended species on further compression. Bulk water behaves differently as it changes from a fully molecular fluid to a dissociated fluid with compression. As a consequence, the volume of silicate melt + water solution is non-ideal at low pressure and becomes ideal above 15 GPa, irrespective of melt composition and water concentration. Also, hydrogen diffusion is decoupled from the rest of ions including oxygen in silicate melts and the associated highly mobile protons make substantial contributions to electrical conduction. Finally, we have demonstrated that the water component controls the stability and conductance of partial melts in the mantle.

**Methods**

First-principles molecuar dynamics simulations of several silicate melt+water systems were performed using the generalized gradients approximation[55] and project augmented wave method[56] as implemented in VASP[57]. All simulations were based on canonical *NVT* ensembles where the number of atoms *N*, volume *V*, and temperature *T* are fixed. The supercells consisted of $32MgSiO_3$ + $16H_2O$ ($N = 208$), $16Mg_2SiO_4 + 8H_2O$ ($N = 136$), and $16Mg_2SiO_4 + 16H_2O$ ($N = 160$) for hydrous silicate melts containing 8.2, 6.0, and 11.4 wt% water (equivalently, 20.0, 14.3 and 25.0 mol% water), respectively. The corresponding water-free supercells involved $32MgSiO_3$ and $16Mg_2SiO_4$. To simulate iron-bearing melts, Mg atoms were substituted with Fe atoms for $x$ = Fe/(Mg+Fe) = 0.25. A plane wave cutoff of 400 eV and Gamma Point Brillouin zone sampling were used. Pulay stress added to the calculated pressure varies between ~3 and ~8 GPa over the

volume range $V/V_0$ = ~1.0 to ~0.4 (where $V_0$ is the zero-pressure volume shown in Table 1) considered in this study.

The input configurations for each melt composition at different volumes were generated at temperatures well above the melting point followed by quenching to desired lower temperatures of 4000, 3000, and 2000 K. The run duration varies between 20 and 80 picoseconds with a time step of 1 femtosecond depending on volume and temperature. The liquid state was confirmed in each case by assuring that the radial distribution functions show no long-range order and the mean square displacement functions show diffusive regime[58]. We also performed a few simulations using the local density approximation[59]. The calculated results were assured to be adequately converged with respect to run duration, time step, and supercell size by performing additional simulations at selected conditions. For comparisons, pure fluid water was simulated using 24 formula units ($N$ = 72), a plane wave cutoff of 600 eV, and a timesetp of 0.5 femtosecond. The applied Pulay stress varies from 0.2 to 0.8 GPa over the six-fold compresson regime considered. Further details about the simulation and data analysis methods can be found in previous publications[58,60].

**Acknowledgements.** This work was supported by National Science Foundation (EAR 1764140, EAR 2001074). The computing resources provided by Louisiana State University High Performance Computing.

## References


1. Hirschmann, M. M. Water, melting, and the deep Earth $H_2O$ cycle. *Rev. Earth Planet. Sci.* **34**, 629–653 (2006).
2. Schmandt, B., Jacobsen, S. D., Becker, T. W., Liu, Z., & Dueker, K. G. Dehydration melting at the top of the lower mantle. *Nature* **344**, 1265-1268 (2014).
3. Karato, S.-I, Karki, B. B. & Park, J. Deep mantle melting, global water circulations and its implications for the stability of the ocean mass. *Prog. Earth Planet. Sci.* **7**, 76 (2020).
4. Matsukage, K. N., Jing, Z. & Karato, S. Density of hydrous silicate melt at the conditions of Earth's deep upper mantle. *Nature* **438**, 488-491 (2005).
5. Sakamaki, T., Ohtani, E., Urakawa, S., Suzuki, A. & Katayama, Y. Measurement of hydrous peridotite magma density at high pressure by X-ray absorption method. *Earth Planet. Sci. Lett.* **287**, 293–297 (2009).
6. Bajgain, S., Ghosh, D.B. & Karki, B.B. Structure and density of basaltic melts at mantle conditions from first-principles simulations. *Nature Comm.* **6**, 8578 (2015).
7. Mookherjee, M., Stixrude, L. & Karki, B. B. Hydrous silicate melt at high pressure. *Nature* **452**, 983-986 (2008).
8. Ni, H., Keppler, H. & Behrens, H. Electrical conductivity of hydrous basaltic melts: implications for partial melting in the upper mantle. *Contrib. Mineral. Petrol.* **162**, 637–650 (2011).
9. Freitas, D. & Manthilake, G. Electrical conductivity of hydrous silicate melts: Implications for the bottom-up hydration of Earth's upper mantle. *Earth Planet. Sci. Lett.*, **523**, 115712 (2019).
10. Sakamaki, T. Density of hydrous magma. *Chem. Geol.* **475**, 135-139 (2017).
11. Dufils, T., Sator, N., Guillot, B. A comprehensive molecular dynamics simulation of hydrous magmatic liquids. *Chem. Geol.* **533**, 119300 (2020).
12. Sakamaki, T., Suzuki, A. & Ohtani, E. Stability of hydrous melt at the base of the Earth's upper mantle. *Nature* **439**, 192-194 (2006).
13. Karki, B.B., Ghosh, D.B., Maharjan, C., Karato, S-I & Park, J. Density-pressure profiles of Fe-bearing $MgSiO_3$ liquid: Effects of valence and spin states, and implications for the chemical evolution of the lower mantle. *Geophys. Res. Lett.* **45**, 3959-3966 (2018a).
14. Agee, C. B. Compressibility of water in magma and the prediction of density crossovers in mantle differentiation. *Phil. Trans. R. Soc.* **366**, 4239-4252 (2008a).
15. Stixrude, L., De Koker, N., Sun, N., Mookherjee, M. & Karki, B. B. Thermodynamics of silicate liquids in the deep Earth. *Earth Planet. Sci. Lett.* **278**, 226–232 (2009).
16. Lizarralde, D., Chave, A., Hirth, G. & Schultz, A. Northeastern Pacific mantle conductivity profile from long-period magnetotelluric sounding using Hawaii-to-California submarine cable data. *J. Geophys. Res.* **100**, 17837-17854 (1995).

17. Toffelmier, D. A. & Tyburczy, J. A. Electromagnetic detection of a 410-km-deep melt layer in the southwestern United States. *Nature* **447**, 991–994 (2007).

18. Baba, K., Utada, H., Goto, T., Kasaya, T., Shimizu, H. & Tada, N. Electrical conductivity imaging of the Phillipine Sea upper mantle using seafloor magnetotelluric data. *Phys. Earth Planet. Inter.* **183**, 44-62 (2010).

19. Manning, C. E. The influence of pressure on the properties and origins of hydrous silicate liquids in Earth's interior. In: Kono, Y., Sanloup, C. (Eds.), *Magmas Under Pressure: Advances in High-Pressure Experiments on Structure and Properties of Melts*, Cambridge, 83–114 (2018).

20. Ochs, F. A. & Lange, R. A. The density of hydrous magmatic liquids. *Science* **283**, 1314-1317 (1999).

21. Bouhifd, M. A., Whittington, A. & Richet, P. Densities and volumes of hydrous silicate melts: new measurements and predictions. *Chem. Geol.* **418**, 40–50 (2015).

22. Gaillard F. Laboratory measurements of electrical conductivity of hydrous and dry silicic melts under pressure. *Earth Planet. Sci. Lett.* **218**, 215-228 (2004).

23. Guo X., Bin L., Ni H. & Mao Z. Electrical conductivity of hydrous andesitic melts pertinent to subduction zones. *J. Geophys. Res. Solid Earth* **122**, 1777-1788 (2017).

24. Du, Z., Deng, J., Miyazaki, Y., Mao, H.-k, Karki, B.B. & Lee, K.L.M. Fate of hydrous Fe-rich silicate melt in Earth's deep mantle. *Geophys. Res. Lett.* **46**, 9466-9473 (2019).

25. Karki, B. B., Ghosh, D. & Banjara, D. Mixed incorporation of carbon and hydrogen in silicate melts under varying pressure and redox conditions. *Earth Planet. Sci. Lett.* **549**, 116520 (2020).

26. Yuan, L., Steinle-Neumann, G. & Suzuki, A. Structure and density of $H_2O$-rich $Mg_2SiO_4$ melts at high pressure from ab initio simulations. *J. Geophys. Res.: Solid Earth* **125**, e2020JB020365 (2020).

27. Encrenaz, T. Water in the solar system. *Annu. Rev. Astron. and Astrophys.* **46**, 57-87 (2008).

28. Baraffe, I., Chabrier, G. & Barman, T. The physical properties of extra-solar planets. *Rep. Prog. Phys.* **73**, 016901 (2010).

29. Millot, M., Coppari, F., Rygg, J. R., Barrios, A. C., Hamel, S., Swift, D. C. & Eggert, J. H. Nanosecond X-ray diffraction of shock-compressed superionic water ice. *Nature* **569**, 251-255 (2019).

30. Mattsson, T. R. & Desjarlais, M. P. Phase diagram and electrical conductivity of high energy density water from density functional theory. *Phys. Rev. Lett.* **97**, 017801 (2006).

31. Jing, Z. & Karato, S. Effect of $H_2O$ on the density of silicate melts at high pressures: static experiments and the application of a modified hard-sphere model of equation of state. *Geochim. Cosmochim. Acta* **85**, 357–372 (2012).

32. French, M., Mattsson, T. R., Nettelmann, N. & Redmer, R. Equation of state and phase diagram of water at ultrahigh pressures as in planetary interiors. *Phys. Rev. B* **79**, 054107 (2009).

33. Pitzer, K. S. & Sterner, S. M. Equations of state valid continuously from zero to extreme pressures for $H_2O$ and $CO_2$. *J. Chem. Phys.* **101**, 3111–3116 (1994).

34. Withers A. C., Kohn S. C., Brooker R. A. & Wood B. J. A new method for determining the P-V-T properties of high-density $H_2O$ using NMR: Results at 1.4-4.0 GPa and 700-11°C. *Geochim. Cosmochim. Acta* **64**, 1051-1057 (2000).

35. Sanchez-Valle, C., Mantegazzi, D., Bass, J. D. & Reusser, E. Equation of state, refractive index and polarizability of compressed water to 7 GPa and 673 K. *J. Chem. Phys*. **138**, 054505 (2013).

36. Sugimura, E., Iitaka, T., Hirose, K., Kawamura, K., Sata N. & Ohishi, Y. Compression of $H_2O$ ice to 126 GPa and implications for hydrogen bond symmetrization: Synchrotron x-ray diffraction measurements and density functional calculations. *Phys. Rev. B.* **77**, 214103 (2008).

37. Ochs, F. A., Lange, R. A. The partial molar volume, thermal expansivity, and compressibility of $H_2O$ in $NaAlSi_3O_8$ liquid: new measurements and an internally consistent model. *Contrib. Mineral. Petrol.* **142**, 235–243 (1997).

38. Makhluf, A. R., Newton, R. C. & Manning, C. E. Hydrous albite magmas at lower crustal pressure: new results on liquidus $H_2O$ content, solubility, and $H_2O$ activity in the system $NaAlSi_3O_8$-$H_2O$-NaCl at 1.0 GPa. *Contrib. Mineral. Petrol.* **171**, 75 (2016).

39. Malfait, W. J., Seifert, R., Petitgirard, S., Mezouar, M., Sanchez-Valle, C. The density of andesitic melts and the compressibility of dissolved water in silicate melts at crustal and upper mantle conditions. *Earth Planet. Sci. Lett.* **393**, 31–38 (2014a).

40. Malfait, W. J., Seifert, R., Perirgirard, S., Perrillat, J. P., Mezouar, M., Ota, T., Nakamura, E., Lerch, P., Sachez-Valle, C. Supervolcano eruptions driven by melt buoyancy in large silicic magma chambers. *Nat. Geosci.* **7**, 122–125 (2014b).

41. Agee, C. B. Static compression of hydrous silicate melt and the effect of water on planetary differentiation. *Earth Planet. Sci. Lett.* **265**, 641–654 (2008b).

42. Seifert, R., Malfait, W. J., Petitgirard, S. & Sanchez-Valle, C. Density of phonoliticmagmas and time scales of crystal fraction in magma chambers. *Earth Planet. Sci. Lett.* **381**, 12–20 (2013).

43. Bureau H. & Keppler H. Complete miscibility between silicate melts and hydrous fluids in the upper mantle: experimental evidence and geochemical implications. *Earth Planet. Sci. Lett.* **165**, 187-196 (1999).

44. Papale, P., Moretti, R. & Barbato, D. The compositional dependence of the saturation surface of $H_2O$ + $CO_2$ fluids in silicate melts. *Chem Geol* **229**, 78–95 (2006).

45. Mibe, K, Kanzak, M., Kawamato, T., Kyoka, N. M., Fei, Y. & Ono, S. Second critical endpoint in the peridotite-$H_2O$ system. *J. Geophys. Res. Solid Earth* **112**, B03201 (2007).

46. Karki, B. B., Bhattarai, D., Mookherjee, M. & Stixrude L., Visualization-based analysis of structural and dynamical properties of simulated hydrous silicate melt. *Phys. Chem. Mineral.* **37**, 103-117 (2010).

47. Karki, B. B. & Stixrude, L. First-principles study of enhancement of transport properties of silica melt by water. *Phys. Rev. Lett.* **104**, 744-751 (2010).

48. Stolper, E. The speciation of water in silicate melts. *Geochim. Cosmochim. Acta* **46**, 2609e2620 (1982)

49. Behrens, H. Water speciation in oxide glasses and melts. *Chem. Geo.* **558**, 119850, (2020).

50. Dziewonski, A. M. & Anderson, D. L. Preliminary reference Earth model. *Phys. Earth Planet. Inter.* **25**, 297-356 (1981).

51. Fei, H. Water content of the dehydration melting layer in the topmost lower mantle. *Geophys. Res. Lett*. **48**, e2020GL090973 (2021).

52. French M., Mattsson T. R. & Redmer R. Diffusion and electrical conductivity in water at ultrahigh pressures. *Phys. Rev. B* **82**, 174108 (2010).

53. Mitchell, A. C. & and Nellis, W. J. Equation of state and electrical conductivity of water and ammonia shocked to the 100 GPa (1 Mbar). *J. Chem. Phys.* **76**, 6273 (1982).

54. Chau, R., Mitchell, A. C., Minich, R. W. & Nellis, W. J. Electrical conductivity of water compressed dynamically to pressures of 70–180 GPa (0.7–1.8 Mbar). *J. Chem. Phys.* **114**, 1361–1365 (2001).

55. Perdew, J. P., Burke, K. & Ernzerhof, M. Generalized gradient approximation made simple. *Phys. Rev. Lett.* **77**, 3865-3868 (1996).

56. Kresse, G. & Joubert, D. From ultrasoft pseudopotentials to the projector augmented-wave method. *Phys. Rev. B* **59**, 1758-1975 (1999).

57. Kresse, G. & Furthmuller, J. Efficiency of ab-initio total energy calculations for metals and semiconductors using a plane-wave basis set. *Comp. Mater. Sci.* **6**, 15-50 (1996).

58. Karki, B.B., Ghosh, D.B. & Bajgain, S.K. Simulation of silicate melts under pressure. In: Kono, Y. & Sanloup, C. (Eds.), *Magmas Under Pressure: Advances in High-Pressure Experiments on Structure and Properties of Melts*, pp. 419-453, Elsevier. (2018b).

59. Ceperley, D. M. & Alder, B. J. Ground-state of the electron-gas by a stochastic method. *Phys. Rev. Lett.* **45**, 566–569 (1980).

60. Bhattarai, D. & Karki, B. B., Atomistic visualization: space–time multiresolution integration of data analysis and rendering. *J Mol Graph Model* **27**, 951–968 (2009).

# Figures

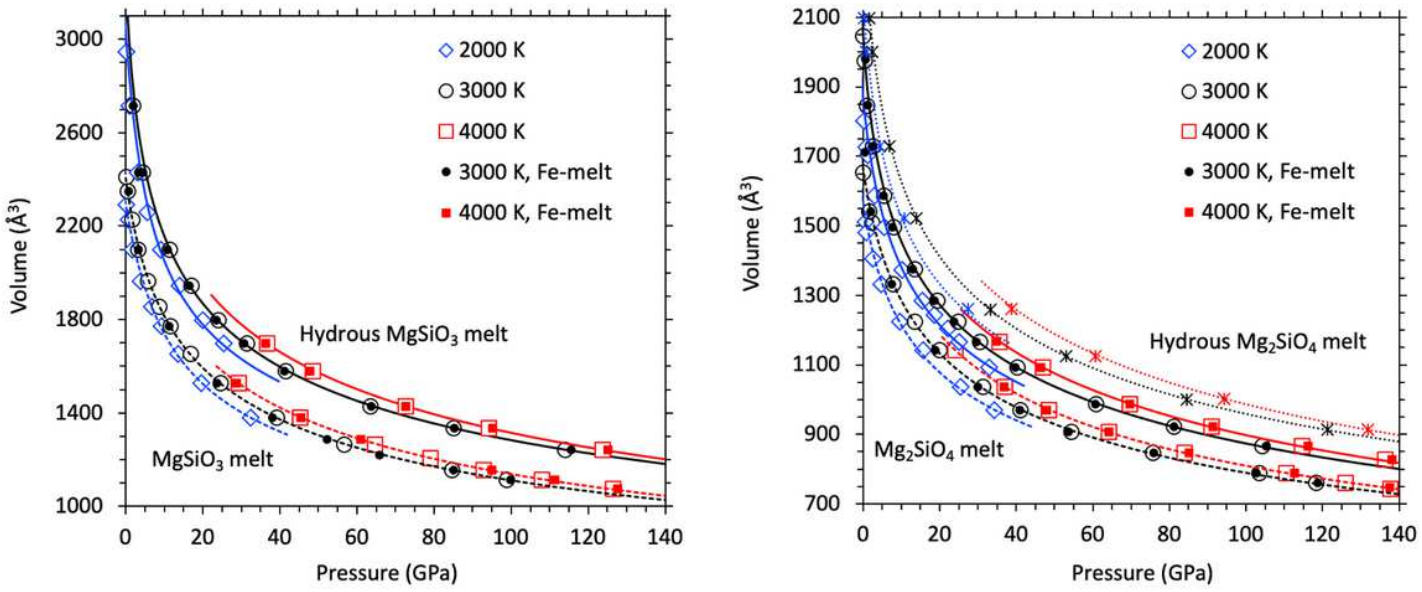


**Figure 1**

The volume-pressure profiles of hydrous MgSiO3 (left) and Mg2SiO4 (right) melts compared to their dry counterparts at 2000 K (blue diamonds), 3000 K (black circles) and 4000 K (red squares). Curves represent the equation of state fits using Eq. 1 and 2. The supercells consist of 32MgSiO3+16H2O (8.2 wt% water) and 16Mg2SiO4+8H2O (6.0 wt% water) and corresponding iron-bearing phases at 3000 and 4000 K (small solid symbols). Also shown are the results for 16Mg2SiO4+16H2O (11.4 wt% water) at three temperatures (asterisks and dotted curves).

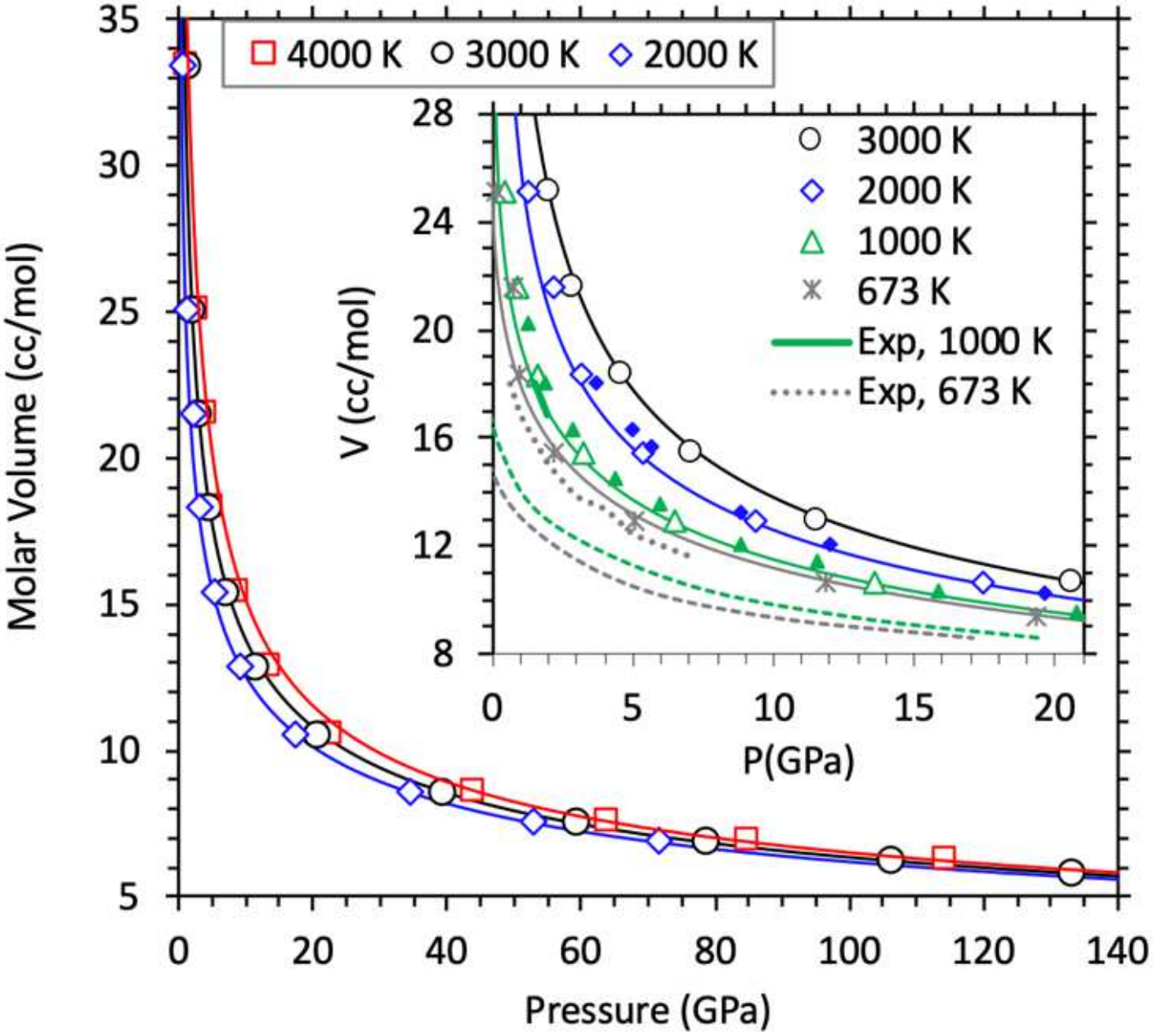


**Figure 2**

Volume-pressure relationships of pure liquid water at 2000, 3000 and 4000 K. Symbols represent the calculated values and curves represent the corresponding equation of state fits. The inset compares our calculated results (symbols and curves) with the available low-pressure experimental data at 673 and 973 K34,35 and the previous calculations shown by small solid triangles and diamonds32. Also shown are the LDA results at 673 and 1000 K (green and gray dashed lines) which are shifted downward with respect to both the GGA and experimental results.

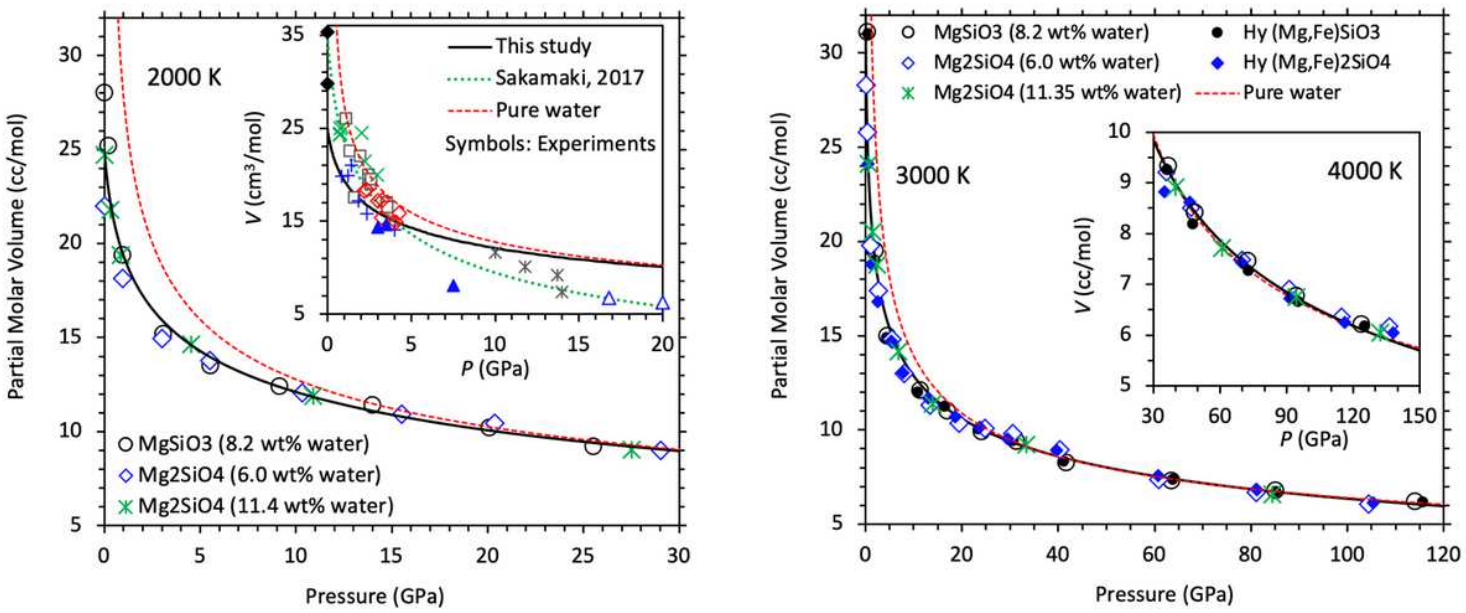


## Figure 3

Calculated partial molar volume of water in hydrous MgSiO3 enstatite melt (8.2 wt% water) and Mg2SiO4 forsterite melts (6.0 and 11.4 wt% water) at 2000 K and in their iron-free and iron-bearing phases (Mg1-xFexSiO3 and Mg2(1-x)Fe2xSiO4 for x = 0 and 0.25) at 3000 and 4000 K as a function of pressure. Also shown is the equation of state fit to all melt results together at each temperature (solid curve) compared to the calculated equation of state for pure water (red dashed curve). The inset on left shows the experimental data on the partial molar volume of water in several silicate melts in the temperature range 1273 to 2473 K projected to 2000 K using the model of Sakamaki10. Different symbols represent different melt compositions, plus: andesite39, solid triangle: basalt12, square: granite40, open triangle: komotiite41, open diamond: peridotite5, cross: phonolite42, and asterisk: ultramafic4,31; solid diamond: hydrous silicate melts at 0 GPa20,21.

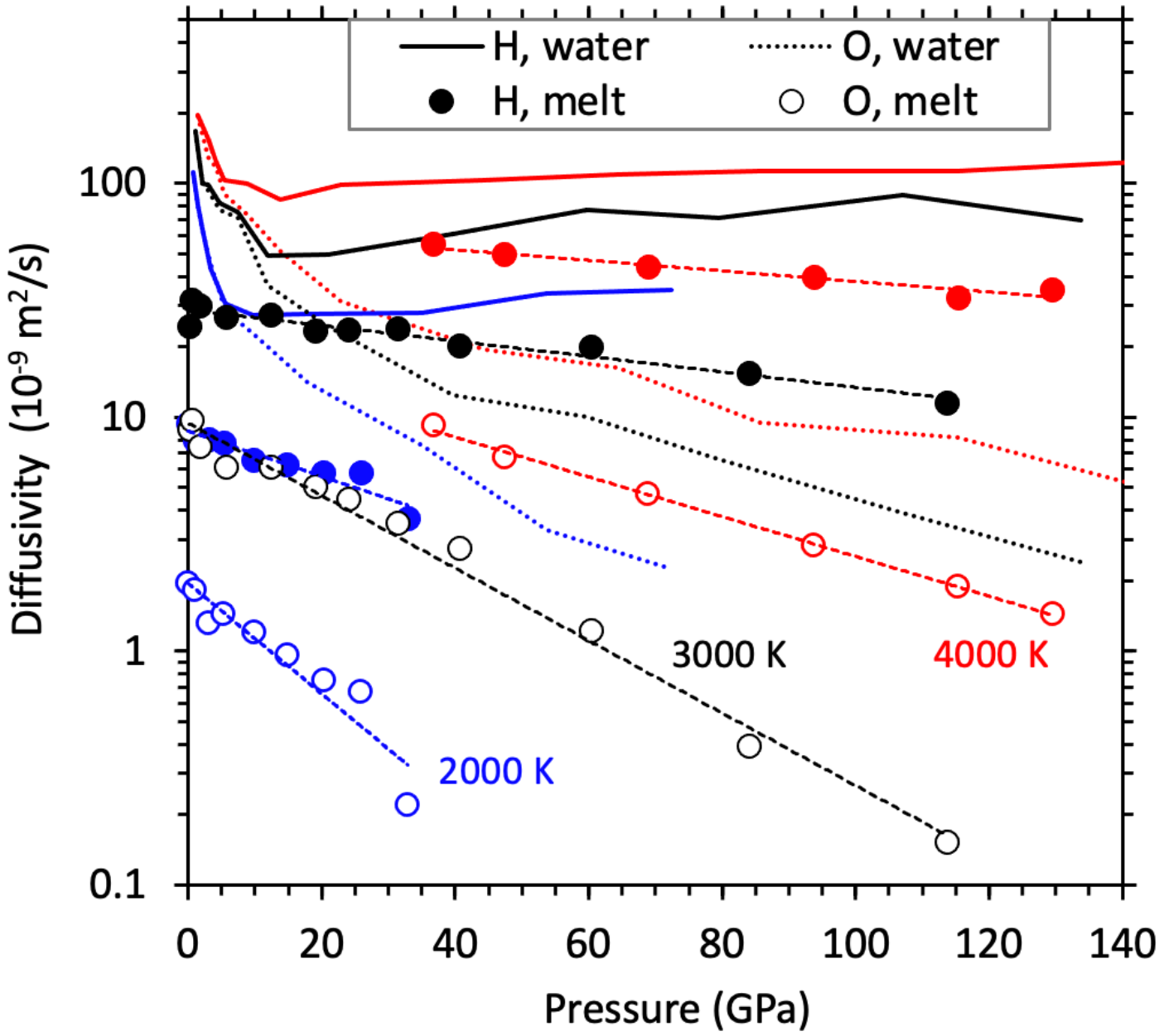


**Figure 4**

Diffusivity-pressure profiles of hydrogen and oxygen of hydrous silicate melts (symbols) taken as averages over five melt compositions at 2000 K (blue), 3000 K (black), and 4000 K (red). Their Arrhenius trends are represented by straight dashed lines. Also shown are the diffusivity results of pure water (solid curves for H and dotted curves for O).

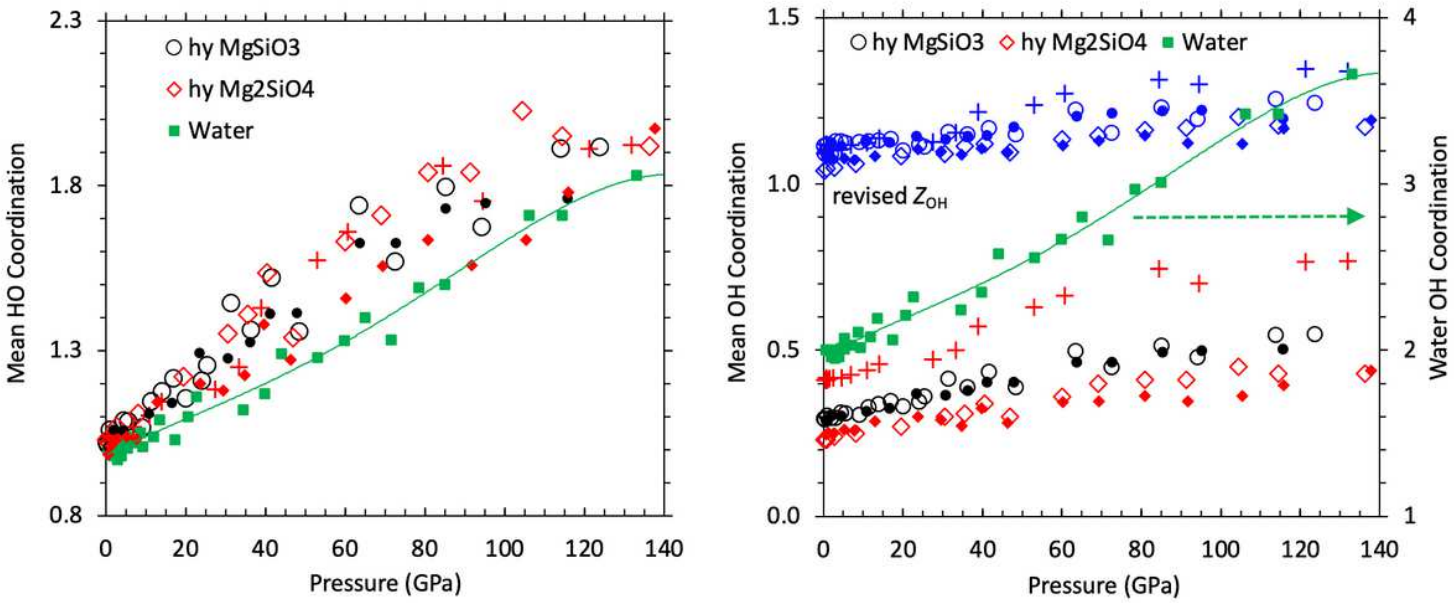


## Figure 5

Mean H-O and O-H coordination numbers of hydrous MgSiO3 with 8.2 wt% water (circles) and Mg2SiO4 with 6.0 wt% water (diamonds) and 11.4 wt% water (pluses) compared to those of water (solid squares). The revised ZOH (right) represents the mean coordination number evaluated by considering only oxygen atoms that contribute to the coordination. The results for the corresponding iron-bearing phases are shown by small solid symbols.

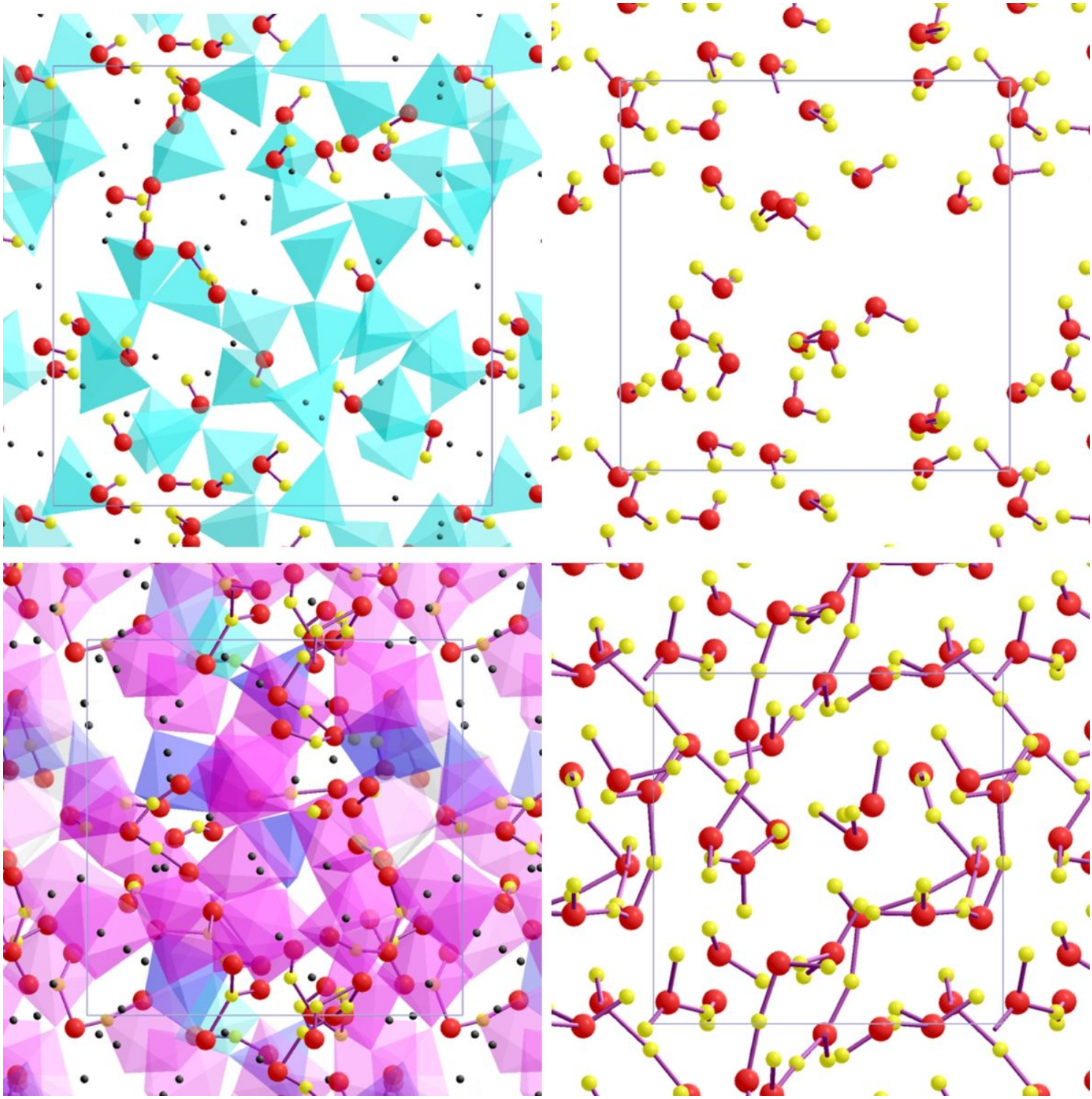

**Figure 6**

Visualization snapshots of hydrous silicate melt (32 MgSiO3 + 16 H2O) and bulk water (24 H2O) at low and high pressures59. The hydrous melt consists of mostly hydroxyls with one H2O molecule and one -O-H-O- bridge at 0.2 GPa and 2000 K (top-left). It shows fewer hydroxyls, many -O-H-O- bridges, and longer sequences (-O-H-O-H-O-, -O-H-O-H-O-H-O-, HO3) at 85.1 GPa and 3000 K (bottom-left). Also shown are the Si-O coordination states (cyan: tetrahedron, blue: pentahedron, magenta: octahedron) and Mg atoms (black dots). The simulated pure water contains only water molecules at 0.7 GPa and 2000 K (top-right).

A highly compressed water (79.4 GPa and 3000 K) contains ten OH2, twelve OH3, and two OH4, which are also interconnected with each other via hydrogen (bottom-right).

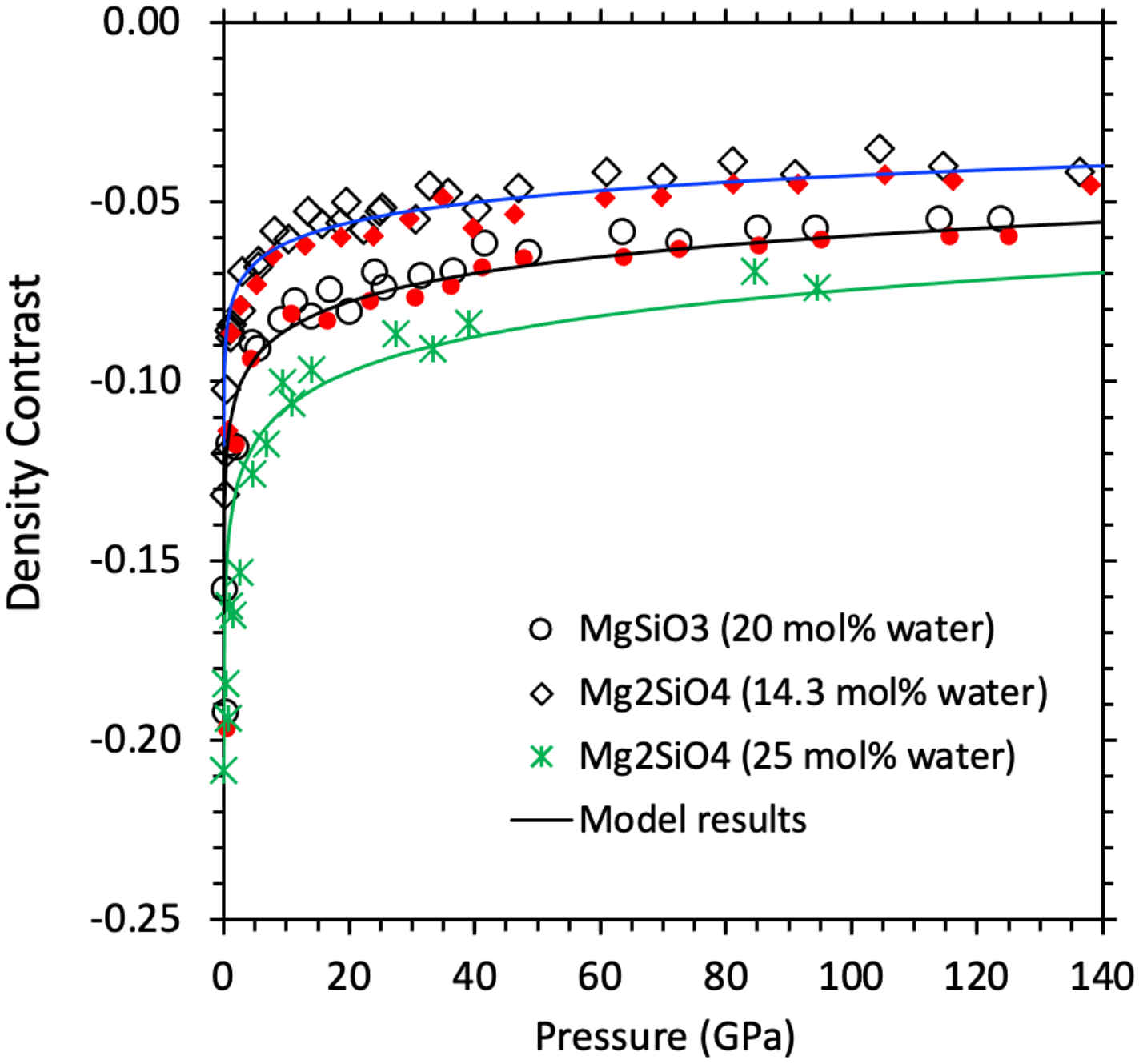


**Figure 7**

Density contrast between dry and hydrous melts for iron-free (open symbols and asterisks) and iron-bearing (filled small symbols) compositions as a function of pressure. The model results using Eq. 4 are shown by curves.

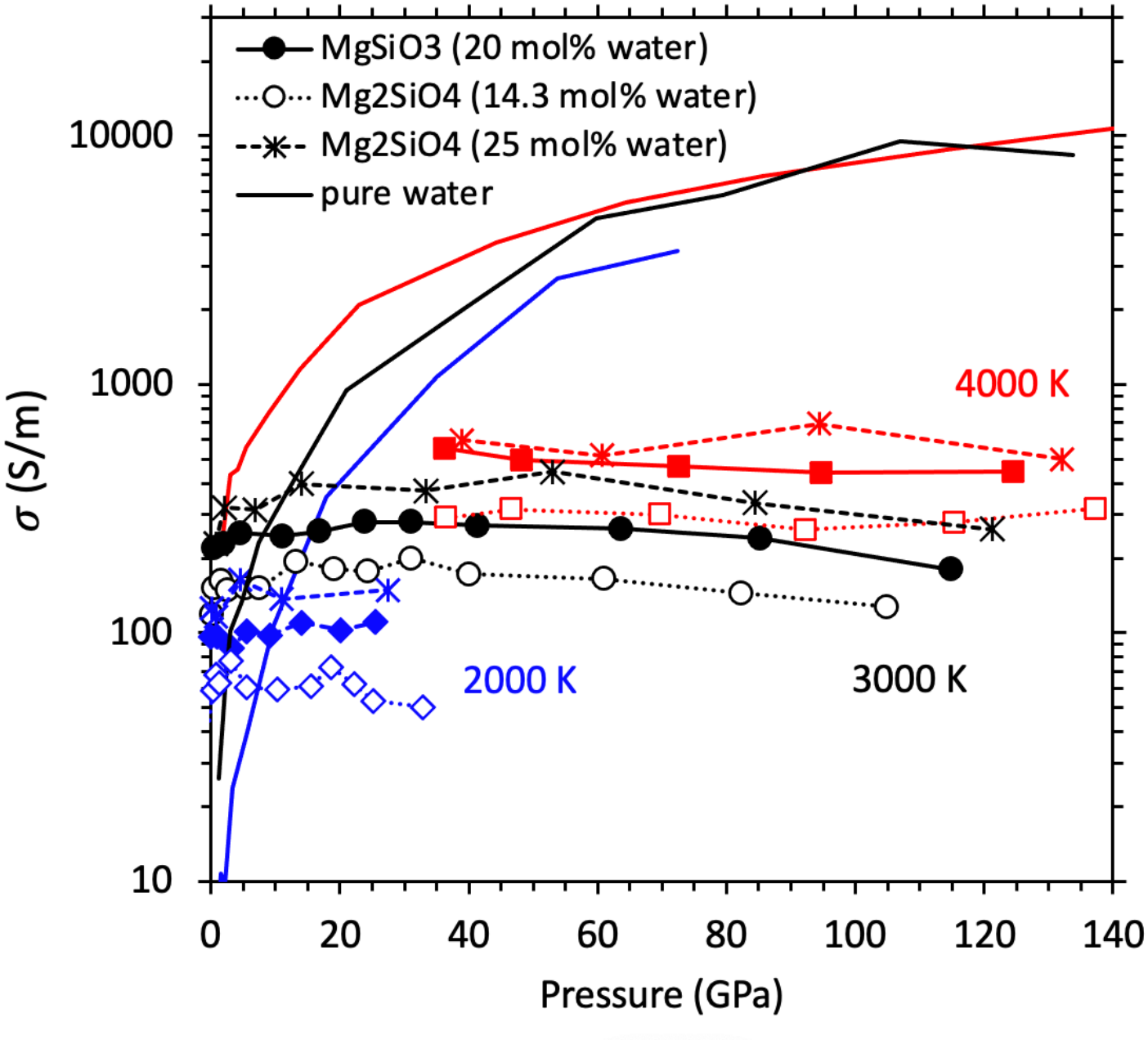


**Figure 8**

Hydrogen-induced electrical conductivity (σ) of hydrous MgSiO3 (filled symbols) and Mg2SiO4 melts (open symbols and asterisks) and bulk water (solid curves) as a function of pressure at different temperatures. The melt conductivity at 3000 and 4000 K represent the averages taken between the iron-free and iron-bearing compositions (iron has almost no influence on the conductivity).

## Supplementary Files

This is a list of supplementary files associated with this preprint. Click to download.

- SI16Feb2021.pdf